Ecological Modelling 331 (2016) 86–99

Contents lists available at ScienceDirect

Ecological Modelling

journal homepage: www.elsevier.com/locate/ecolmodel

A physically coupled end-to-end model platform for coastal ecosystems: Simulating the effects of climate change and changing upwelling characteristics on the Northern California Current ecosystem

James J. Ruzicka[a,*], Kenneth H. Brink[b], Dian J. Gifford[c], Frank Bahr[b]

[a] Cooperative Institute for Marine Resources Studies, Oregon State University, Hatfield Marine Science Center, Newport, OR 97365, USA
[b] Woods Hole Oceanographic Institution, Woods Hole, MA 02543, USA
[c] Graduate School of Oceanography, University of Rhode Island, Narragansett, RI 02882, USA

ARTICLE INFO

Article history:
Available online 15 February 2016

Keywords:
ECOTRAN
ECOPATH
Intermediate complexity model
Northern California Current
Upwelling
Climate change

ABSTRACT

We describe a spatially explicit, intermediate complexity end-to-end model platform that integrates physical, trophic, and nutrient cycling processes. A two-dimensional advection and mixing model drives nitrate input into the model continental shelf domain, the transport of nutrients and plankton between sub-regions, and the export of nutrients and plankton from the model domain. Trophic relationships are defined by classical mass-balanced food web model techniques (e.g., ECOPATH). Inclusion of nitrate and ammonium nutrient pools and bacterial recycling of detritus allows consideration of alternate "new" vs. "recycled" production regimes. The model platform was applied to the Northern California Current (NCC) shelf ecosystem. Seasonal upwelling of nutrients along the coast is the primary driver of NCC productivity, however the characteristics of upwelling vary considerably between years and are expected to change into the future as a result of global climate change. The model was run under alternate physical driver scenarios to examine the effects of changing upwelling characteristics on the production and spatial distribution of functional groups across all trophic levels. Productivity on the shelf had a dome-shaped relationship with upwelling strength. As the intensity of individual upwelling events increased, productivity increased throughout the food web. However, strong upwelling had a detrimental effect when the physical export of plankton exceeded the capacity of phytoplankton to exploit higher nutrient supply rates and the capacity of zooplankton to exploit higher phytoplankton production. As the duration of individual upwelling events increased (an implication of some climate change scenarios) model simulations predicted an overall reduction of productivity at all trophic levels and a shift in the size composition of the phytoplankton community, especially within the nearshore region.

1. Introduction

Ocean ecosystems are as much defined by their physical characteristics as they are by their species composition and community interactions. A central issue in understanding ecosystem dynamics is the role of the physical context in determining community structure, productivity, and response to natural and anthropogenic perturbations. Model-based comparisons of the dynamics of different ocean ecosystems (e.g., Gaichas et al., 2009; Ainsworth et al., 2011; Ruzicka et al., 2013) focus on the role of food web structure – the network of trophic relationships and energy flow pathways through pelagic and benthic communities. With the development of food web modelling platforms like ECOPATH with ECOSIM (Pauly et al., 2000; Christensen and Walters, 2004), analyses and simulations of variable trophic interactions, resource management actions, and effects of changing community composition have been standardized. The addition of physical processes to trophic models increases the level of complexity. For example, ATLANTIS models (Fulton et al., 2004; Link et al., 2010) link 3-dimensional physical ocean models, NPZD plankton production models of the lower food web, and non-linear prey-predator relationships among higher trophic levels to build complete end-to-end model systems – describing both the physical transport of nutrients and biomass as well as the production and transfer of biomass throughout the food

* Corresponding author.
E-mail address: jim.ruzicka@oregonstate.edu (J.J. Ruzicka).

http://dx.doi.org/10.1016/j.ecolmodel.2016.01.018
0304-3800/

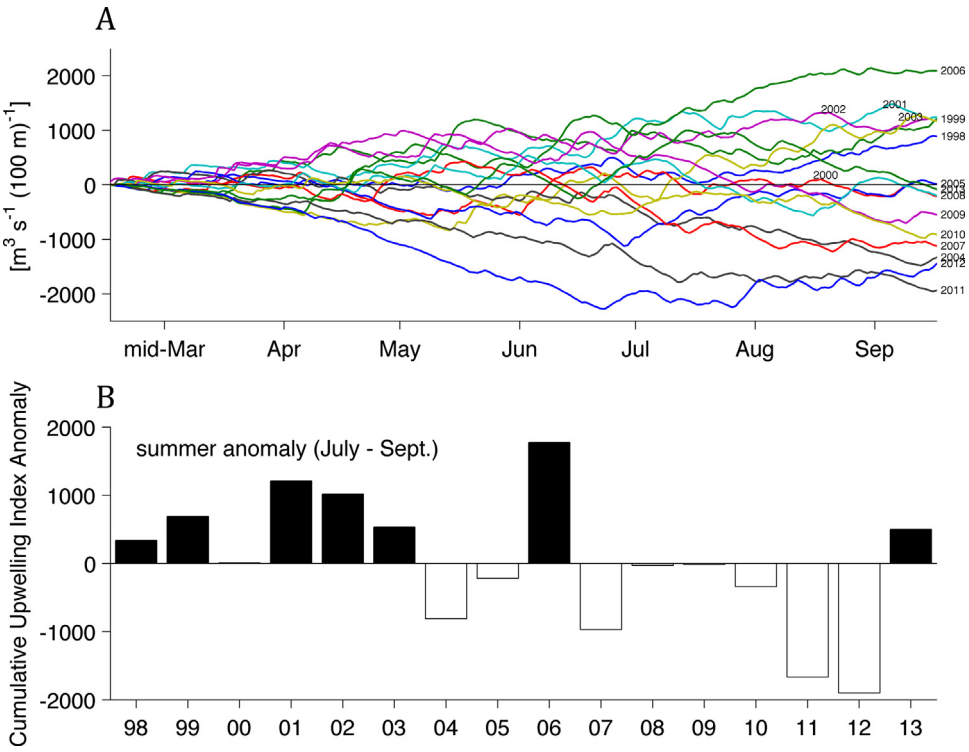

Fig. 1. The cumulative upwelling index anomalies off the central Oregon coast between 1998 and 2013. (A) Daily cumulative anomaly, (B) Cumulative summer anomaly (July–Sept.).

web, from the input of nutrients, to fisheries production, and finally to detritus and nutrient recycling. Currently, these highly complex end-to-end model systems are used more for exploration of individual ecosystems than as frameworks for comparative systems analysis.

We present the theoretical framework for a spatially explicit, intermediate complexity end-to-end ecosystem model platform that integrates physical and biological processes. The ultimate goal of this model framework is to define physical and biological components with sufficient generality to allow standardized comparisons among diverse ecosystem types (e.g., upwelling, downwelling, shallow bank, or semi-enclosed sea) but still encompass the essential physics and trophic structure of each ecosystem. As a test of model behaviour, we apply this framework to the Northern California Current (NCC), an eastern boundary current upwelling ecosystem.

The defining chemical, biological and physical features of coastal upwelling systems are the wind-driven input of nutrient-rich sub-surface waters into the euphotic zone along the coastline, seasonally high rates of primary and secondary productivity, and the lateral transport of plankton production across the shelf (Huyer, 1983; Strub et al., 1987). The characteristics of NCC upwelling – the seasonality, intensity, and duration of upwelling and relaxation events – have varied greatly between years (Bograd et al., 2009; Fig. 1) and are expected to further deviate from current conditions with the progress of global climate change (Bakun, 1990). Changing seasonal and event-scale upwelling characteristics drive variability in the productivity, taxonomic composition, and spatial distribution of the phytoplankton community (Wilkerson et al., 2006; Du et al., 2015) with consequences to the greater consumer food web it supports (e.g., Fisher and Pearcy, 1988). Here, we use the integrated physical-biological model platform to simulate NCC ecosystem response, across all trophic levels, to changing physical conditions. In particular, we investigate the effects of alternate upwelling intensities and event durations.

2. Methods

In the following sections, we first describe the theoretical framework for the construction of an intermediate complexity, physically coupled end-to-end (E2E) model built upon traditional ECOPATH food web models. We then describe an application of this model platform to the Northern California Current upwelling ecosystem and use the model to simulate ecosystem response to changing upwelling conditions: upwelling strength and upwelling event duration.

2.1. Theoretical framework – generic model structure

2.1.1. Overview

A physically coupled end-to-end (E2E) model describing energy or biomass transfer through an ecosystem has four essential components: (1) a description of the network of trophic interactions between all living functional groups, (2) defined primary production rates, (3) a description of recycling processes and rates, and (4) a description of the physical environment defining the transport of material within and across ecosystem boundaries and conditions controlling physiological rates. Although taxonomic resolution, demographic resolution, and spatial-temporal resolution vary greatly among models and applications, all E2E models incorporate these essential components. The E2E framework presented here is applicable to shelf ecosystems, where the dominant physical fluxes between explicitly defined subregions (Fig. 2) may be described in 2-dimensions: cross-shelf advection, horizontal and vertical mixing, and particle sinking. Because the underlying food web model is built by averaging trophic interactions over large alongshore distances, we make the simplifying assumption that the system is reasonably 2-dimensional over these alongshore scales (e.g., Lentz, 1987).

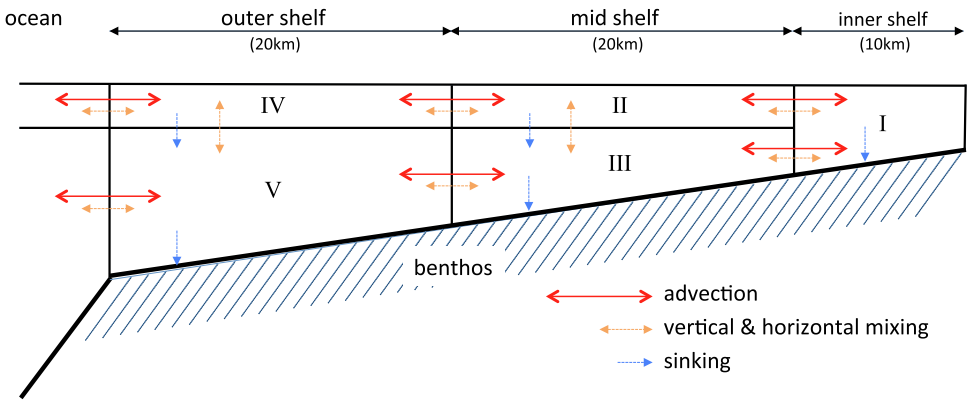

Fig. 2. The spatial arrangement of sub-regions for the Northern California Current coupled physical-biological model. Arrows indicate advective fluxes driven by coastal upwelling, vertical mixing fluxes, horizontal mixing fluxes, and phytoplankton sinking fluxes.

2.1.2. Food web structure

The end-to-end food web model (defined by matrix A_{cp}, Eq. (4)) describes the transfer of biomass between all producer (p)–consumer (c) pairs, flow of egestion and senescent biomass to detritus pools, and the recycling of nutrients via bacterial metabolism of detritus. The underlying network of trophic interactions within the model is constructed using established ECOPATH techniques. Rates of biomass transfer between all producer and consumer groups are inferred from the estimated predation demands of sequentially lower trophic level consumers upon each of their prey (Christensen and Walters, 2004):

$$Q_{pc} = D_{pc} \cdot q_c \tag{1}$$

where Q_{pc} = consumption matrix; consumption rate of each consumer c upon each producer p, D_{pc} = diet matrix; the fraction of each producer p in the diet of each consumer c, and q_c = consumption rate of consumer c. The consumption rate of each consumer q_c is a function of its production rate p_c, respiration rate in terms of metabolized biomass m_c, and assimilation efficiency ae_c (ae_c = 1 – egested fraction of consumption):

$$q_c = \frac{p_c + m_c}{ae_c}. \tag{2}$$

The production rate of each group p_p is calculated within ECOPATH from a system of linear equations that define production as the sum of predation and fishery harvest pressure, net emigration, senescence (non-predation mortality), and biomass accumulation rates:

$$b_p\left(\frac{p}{b}\right)_p = \sum_c b_c\left(\frac{q}{b}\right)_c D_{pc} + b_p\left(\frac{p}{b}\right)_p\left(1 - ee_p\right) + im_p + ba_p \tag{3}$$

where b = biomass, (p/b) = intrinsic production rate, production rate $p = b\cdot(p/b)$, (q/b) = intrinsic consumption rate, consumption rate $q = b\cdot(q/b)$, $\sum_c b_c(q/b)_c D_{pc}$ = predation pressure on producer p (includes fishery pressure where b = harvest and q/b = (discard + harvest)/harvest), ee = ecotrophic efficiency (fraction of group production used within the living ecosystem and not "lost" to detritus as senescence), im = net emigration into the model domain (im = immigration – emigration), ba = biomass accumulation rate.

The ECOPATH expression of the food web as a consumer → producer map of consumption demands Q_{pc} is then re-expressed as a producer → consumer map of production fate A_{cp} following the ECOTRAN technique of Steele and Ruzicka (2011):

$$A_{cp} = \frac{D_{pc}q_c}{\sum_c D_{pc}q_c} \tag{4}$$

where A_{cp} = production matrix; fraction of total production of each producer p consumed by each consumer c. Matrix A_{cp} is expanded to represent the bioenergetic budget of each consumer by including egestion flow to detritus pools and metabolized biomass flow to nutrient pools added as explicitly defined functional groups. Nutrients are supplied to the model via external input mediated by defined physical processes (Eq. (5)) and via nutrient recycling mediated by bacterial metabolism of detritus and, to a lesser extent, by consumer metabolism. The end-to-end expression of the food web A_{cp} is donor-driven; nutrient uptake by primary producers drives ecosystem production.

Direct modifications of E2E matrix A_{cp} may be used to quantify the consequences of structural energy flow rearrangements – as from changes to the abundance, physiology, or diet of any sub-set of functional groups (Ballerini et al., 2014; Treasure et al., 2015). E2E matrix A_{cp} may also be used in dynamic simulations, allowing for compensatory re-adjustments of community composition and food web structure over time (Steele, 2009):

$$\frac{dq_p}{dt} = r_p\left[te_p\left(\sum_p Q_{cp} + i_p\right) - \sum_c Q_{cp} + \Lambda_p + (ba - im)\right] \tag{5}$$

where q_p = consumption rate of group p, r_p = intrinsic consumption rate $r = (q/b)$, te_p = transfer efficiency of consumption to next higher trophic level (te = 1 for all groups except benthic detritus), $\sum_p Q_{cp}$ = total consumption rate by group p, i_p = external input rate of driver group p (NO_3^-) to model domain (does not define export, i.e., $i_p \geq 0$), $\sum_c Q_{cp}$ = total predation rate upon of group p, Λ_p = net physical transport rate of group p across model domain boundaries (see Section 2.1.3). The consumption matrix Q_{cp} in Eq. (5) is recalculated at each time-step as

$$Q_{cp} = F_{cp} \cdot (A_{cp} \cdot q_p) \tag{6}$$

where q_p is the consumption rate of group p at time t. F is the functional response between producers and consumers (Steele, 2009; Steele and Ruzicka, 2011):

$$F_{cp} = \frac{(1 + m_p)\cdot q_c}{(m_p \cdot q_{c\,at\,t=0}) + q_c}. \tag{7}$$

F_{cp} is analogous to a foraging arena model as used within ECOSIM (Christensen and Walters, 2004), where the ingestion rate of the predator is a function of predator density rather than of prey density. The term m_p is a functional response modifier corresponding to the vulnerability term in a foraging arena model. Prey–predator relationships are linear (F_{cp} = 1) when m_p = 0. When m_p = 1, the consumer half-saturation ingestion rate equals the initial conditions defining the mass-balanced food web, the ECOSIM default condition; and as $m_p \to \infty$, the function begins to approximate the

quadratic form in which ingestion rate will not become satiated (Steele, 2009).

2.1.3. Physical structure

The net physical flux of any functional group across model domain or sub-region boundaries (Fig. 2) may be treated in the same manner as a consumption gain or predation loss term (Eq. (5)). Physical flux is a function of the volumetric flux rates across sub-region boundaries, biomass densities within source sub-regions, and volumes of destination sub-regions. For any group p within a sub-region d:

$$\Lambda_{pd} = \frac{\sum_s (\Phi_{ds} \cdot B_{ps})}{V_d} \quad (8)$$

where Λ_{pd} = net physical flux of group p into sub-region d (biomass density per unit time), Φ_{ds} = net volume flux rate from sub-region s to sub-region d (volume per unit time), B_{ps} = biomass density of group p in sub-region s (biomass per unit volume), $\Phi_{ds} \cdot B_{ps}$ = flux of biomass p per unit time between sub-regions s and d, V_d = volume of destination sub-region d. The net volumetric flux rate Φ_{ds} across the lateral or vertical boundary between sub-regions d and s is the sum of advective fluxes (δ_{ds}), vertical turbulent mixing (β_{ds}), horizontal turbulent mixing (γ_{ds}), and particle sinking (θ_{ds}):

$$\Phi_{ds} = \delta_{ds} + \beta_{ds} + \gamma_{ds} + \theta_{ds}. \quad (9)$$

2.2. Application to the Northern California Current upwelling ecosystem

2.2.1. The Northern California Current food web

The Northern California Current upwelling ecosystem model covers the region from the southern Oregon border (42.00° N) to Cape Flattery, Washington (48.34° N) and cross-shelf from the coastline to the shelf break (approx. 50 km oceanward). The food web model, including nutrient and detritus cycling pathways is described in Ruzicka et al. (2012), and the full parameter set is provided in the Appendix. The model describes the trophic connections between phytoplankton (2 size classes), zooplankton (10 functional groups), gelatinous zooplankton (3 groups), pelagic fishes and squids (30 groups), benthic invertebrates (11 groups), demersal fishes (7 groups), seabirds (8 groups), marine mammals (7 groups), fisheries (17 gear groups), eggs (2 pools), detritus (3 pools), and nutrients (3 pools).

Biomass flows to pelagic and benthic detritus pools were defined separately for faeces and for senescent biomass, based upon the general size and life-history of individuals within each functional group (Appendix Table A8). Non-consumed phytoplankton production is the largest contributor to detritus. Phytoplankton mortality was described by two terms: senescence mortality as defined in the NCC ECOPATH model (Appendix Table A1) and the cell sinking rate (see Section 2.2.2). Bacterial metabolism of pelagic and benthic detritus was assumed to be 50% of the detritus production rate. Unconsumed or un-metabolized pelagic detritus flows to the benthic detritus pool. Benthic detritus was recycled back into the ecosystem (via bacterial metabolism and consumption by metazoans) with a default transfer efficiency of $te = 0.75$ (Eq. (5), see also Section 2.3).

All analyses presented in this study used linear prey–predator relationships for zooplankton and benthic invertebrate consumers ($m_p = 0$, Eq. (7)) and used non-linear relationships for mid- and upper trophic level consumers analogous to ECOSIM default conditions ($m_p = 1$). However, nutrient uptake by diatoms and flagellates was modelled using Michaelis–Menten uptake functions and parameters modified from plankton models developed for the Oregon coast (Newberger et al., 2003; Ruzicka et al., 2011). The physically coupled end-to-end (E2E) ecosystem model was run under 432 alternate parameter set combinations. Each parameter set was evaluated against bi-weekly observations of surface chlorophyll and depth-integrated copepod biomass (to 100 m) along the central Oregon shelf Newport Hydrographic (NH) Line (44.67° N). Details of NH Line methodology are provided by Peterson and Miller (1975), Peterson et al. (2002), and Peterson and Keister (2003). Conversion from chlorophyll to nitrogen biomass was made using standardized conversion factors: Chl a:N = 2.19 mg Chl a mmoles N^{-1} for diatoms (Dickson and Wheeler, 1995), and Chl a:N = 0.84 mg Chl a mmoles N^{-1} for flagellates (Chan, 1980). Evaluation criteria were qualitative: co-existence of both phytoplankton functional groups across seasons and over years, appropriate seasonal patterns of phytoplankton group dominance, and error in modelled phytoplankton and copepod biomass relative to time-series and cross-shelf distribution observations. One parameter set was selected for subsequent simulations of ecosystem behaviour under alternate upwelling conditions (see Appendix and Table A11).

Table 1
Model sub-regions and dimensions for the Northern California Current model.

	Sub-region	Horizontal dimension	Vertical dimension
I	Inner shelf	0–10 km	0–30 m
II	Mid shelf surface	10–30 km	0–15 m
III	Mid shelf sub-surface	10–30 km	15–140 m
IV	Outer shelf surface	30–50 km	0–15 m
V	Outer shelf sub-surface	30–50 km	15–250 m

2.2.2. The Northern California Current physical structure

To account for the physical transport of nutrients, detritus, planktonic, and semi-planktonic groups, the NCC domain is divided into five sub-regions (Fig. 2, Table 1): box I – the inner shelf zone of coastal upwelling, from the coastline oceanward to 10 km; boxes II and III – the mid shelf, 10 to 30 km oceanward; and boxes IV and V – the outer shelf, 30 km to the shelf break at 50 km. Sub-region depths are uniform along their cross-shelf dimensions. The inner shelf domain extends from the surface to the mean ocean depth (30 m). The mean ocean depths across the mid and outer shelf sub-regions are 140 m and 240 m, respectively. The mid and outer shelf sub-regions are divided into surface (boxes II and IV) and sub-surface layers (boxes III and V), defined by an annual mean mixed layer depth of 15 m.

Our goal was to allow easy assimilation of the vertically integrated ECOPATH model structure with the spatially defined physical model. In the present application of the model, boxes I, II, and IV (Fig. 2) represent full, vertically integrated food webs of the inner, mid, and outer shelf zones. Each surface box has its own food web matrix (A_{cp}, Eq. (4)) and includes both pelagic and benthic components. The productivity of each functional group within the inner, mid, and outer shelf zones is driven by the rate of nutrient uptake of phytoplankton in the surface boxes plus physical import and export of lower trophic groups (nutrients, detritus, planktonic, and semi-planktonic groups) across sub-region boundaries. Sub-surface boxes (III and V) are used to account for the physical transport of nutrients and passive particles across the shelf at depth and the loss of sinking phytoplankton from the surface euphotic zone. There is a limited set of trophic exchanges between functional groups allowed within sub-surface boxes III and V: the transfer of phytoplankton to the benthic detritus pool via sinking, the metabolism of detritus by bacteria, and the nitrification of ammonium. Each sub-surface box has its own food web matrix (A_{cp}), but most elements defining trophic exchanges have been set to zero. Phytoplankton that sink or are physically transported into a sub-surface boxes are moribund; they do not assimilate nutrients unless physically transported back to one of the surface boxes.

When a portion of a nutrient pool, or a portion of a detrital or planktonic biomass pool is physically transferred from a surface to a sub-surface box, it becomes temporarily unavailable to the rest of the food web. Nutrients and biomass within sub-surface boxes become available to the rest of the food web through either of three physical processes: upwelling, vertical mixing, or the transfer of sinking particles to the benthic detritus. The surface and sub-surface boxes of the mid (II and III) and outer shelf (IV and V) food webs each share common benthic detritus pools. Finally, note that this model platform does allow for complete separation of pelagic and benthic food webs into separate surface and sub-surface boxes if attention is paid to the vertical distribution and migration of individual functional groups.

Wind-driven upwelling is the dominant physical driver of nutrient input and advection in the NCC. Upwelling transports nutrient rich sub-surface water to inner shelf box I, making nutrients available for phytoplankton uptake, and drives horizontal Ekman transport of nutrients, detritus, planktonic, and semi-planktonic groups across the shelf. Advective flux (δ_{ds}, Eq. (9)) is the daily upwelling index calculated after Schwing et al. (1996):

$$UI = \left(\frac{\tau_y}{f}\right) \cdot \left(\frac{1}{\rho_{water}}\right) \cdot (86,400\,\mathrm{s\ d^{-1}}) \cdot (100\,\mathrm{m\ of\ coastline}) \quad (10)$$

where UI = median daily upwelling index ($m^3\,d^{-1}$, UI < 0 during upwelling), τ_y = north–south wind stress ($kg\,m^{-1}\,s^{-2}$, $\tau_y < 0$ when winds blow to the south), f = Coriolis parameter = $1.025 \cdot 10^{-4}\,s^{-1}$ at 44.65°N, ρ_{water} = seawater density ($1000\,kg\,m^{-3}$). Daily UI values for the central Oregon coast at 45° N 125° W were obtained from the Environmental Research Division, NOAA Southwest Fisheries Science Center (www.pfeg.noaa.gov). The sign of the UI defines the direction of flow through model sub-regions and the relationships between source s and destination d sub-regions at each time step.

Vertical turbulent mixing rates were calculated by closing salinity and temperature property budgets for each model box under the imposition of wind stress. Monthly rates were calculated using climatological salinity and temperature data from GLOBEC and NH Line surveys and climatological wind data from the National Data Buoy Center (buoys NDBC 46041, 46029, and 46050) over years 1984–2009. Vertical mixing takes the form $\beta_{ds} = d_{ps} \cdot HA_d$, where β_{ds} is the volumetric flux rate ($m^3\,s^{-1}$, Eq. (9)), d_{ds} is the turbulent mixing coefficient between sub-regions d and s ($m\,s^{-1}$), and HA_d is the boundary area between sub-regions. The biomass flux into sub-region d due to turbulent vertical mixing (Eq. (8)) is then $\beta_{ds} \cdot (B_{ps} - B_{pd})/V_d$, where $B_{ps} - B_{pd}$ is the difference in the biomass densities of group p in sub-regions d and s. Horizontal mixing (γ_{ds}, Eq. (9)) is negligible compared to horizontal advection and was ignored. Unidirectional sinking flux rates (θ_{ds}, Eq. (9)) for phytoplankton were calculated from defined sinking rates (w_p, Appendix Table A11) multiplied across the horizontal area of each sub-region: $\theta_{ds} = w_p \cdot HA_d$.

Zooplankton groups with low growth rates may not be able to maintain populations upon the shelf under high Ekman transport rates without the action of retention mechanisms that reduce cross-shelf advection (Steele and Ruzicka, 2011). Potential retention mechanisms include diel and ontogenetic vertical migration that decrease the time spent in the surface layer and reduce, or reverse, offshore transport. We simulated the net effect of hypothetical retention mechanisms by applying a scaling factor to the advection rate acting upon each functional group (δ_{ds}, Eq. (9)). Effective advection = $\delta_{ds} \cdot$(1 − retention scaling factor), where the retention scaling factor is 0 for fully planktonic groups and 1 for nektonic or sessile groups. In the general absence of accurate information on appropriate retention scaling factors among coastal planktonic groups, we applied a limited set of values to each simulation in this study (Appendix Table A9). Phytoplankton and microzooplankton were assumed to be purely planktonic, and the retention scaling factor was set to 0. Mesozooplankton groups were assumed to be weakly resistant to advection, and the scaling factor was set to an assumed value of 0.25. Larger macrozooplankton were assumed to resist advection, and the scaling factor was set to 1.

2.2.3. The Northern California Current initial and ocean boundary conditions

The ECOPATH parameter set describing the NCC food web defines the initial biomass of each group within the inner, mid, and outer shelf zones (Appendix Table A1). Observed nitrate concentrations within each sub-region (Table 2) are used to estimate initial primary production rates (using Michaelis–Menten uptake kinetics; see Appendix, Eq. (A1)) that are, in turn, used to drive the model and estimate initial consumption and production rates for every consumer and detritus group.

External input of oceanic nitrate (i_p, Eq. (5)) across the surface and sub-surface oceanic boundaries drives ecosystem production. The external input rate is defined by the physical flux rates across the oceanic boundaries and surface and sub-surface oceanic nitrate concentrations (Table 2). We assume that the biomass of each non-nitrate group is identical on both sides of the model's oceanic boundaries. There is no net oceanic input for any non-nitrate group nor is there dilution due to advection of empty water. This allows advection of biomass out of the model but prevents undefined oceanic processes from affecting the model system (e.g., regional scale transport of large water masses associated with El Niño events or the Pacific Decadal Oscillation).

2.3. Simulations of alternate upwelling strength and event duration

We evaluated the importance of variability in upwelling event strength and duration on the dynamics of groups across all trophic levels and within both pelagic and benthic environments. As a sensitivity analysis, rather than a specific prediction of future conditions, we drove the model system under a range of upwelling intensities and event durations. In the first analysis, the effects of varying upwelling strength were examined by applying scaling factors (0.25–4×) to the amplitude of the 2006–2010 daily upwelling index (UI) time series at 45° N 125° W (www.pfeg.noaa.gov). Scaling factors were applied only during upwelling events. Relaxation (non-upwelling) events and event durations were unaltered. This range of scaling factors spans the 10th to twice the 90th percentile range of individual upwelling event intensities (5.4–60.2 $m^3\,s^{-1}\,(100\,m)^{-1}$) relative to the mean 1967–2014 upwelling season (April–Sept.) event intensity (calculated from the mean daily UI across the duration of individual events).

These scaling factors were also applied to the turbulent vertical mixing rate, which increases linearly with alongshore wind stress and the UI. The advective fluxes are much larger than vertical fluxes due to turbulent mixing, however turbulent mixing contributes to nutrient and biomass exchange between surface and sub-surface waters and thus, the vertical distribution of plankton groups. In the ocean and in the model, changes in vertical distributions and plankton concentrations affect PAR exposure for phytoplankton and affect producer–consumer encounter rates within the plankton community. Finally, as rates of detritus recycling via bacterial metabolism (ammonium production) and, to a lesser degree, via consumption by benthic metazoans are not well known, upwelling simulations were repeated across a broad range of potential benthic detritus transfer efficiencies: te = 0.1, 0.25, 0.5, 0.75, and 0.9. Effects were measured as the final year August biomasses of four indicator groups: copepods and forage fishes are secondary and tertiary producers of the pelagic food web, invertebrate epifuana and semi-demersal fishes (dogfish, *Squalus acanthias*, Pacific hake,

Table 2
Physical model parameters.

Parameter	Value	Units	Source
UI	Time series	$m^3\ s^{-1}\ 100\ m^{-1}$	Coastal Upwelling Index; www.pfeg.noaa.gov
f	$1.025{\cdot}10^{-4}$	s^{-1}	Coriolis parameter at 44.65°N
τ_y	Time series	$kg\ m^{-1}\ s^{-2}$	North-South wind stress; $\tau_y = \rho_{air} \cdot C_d \cdot \vec{v}_y \cdot \lvert W \rvert$
ρ_{air}	1.220	$kg\ m^{-3}$	Air density, (Schwing et al., 1996)
C_d	≥0.0011		Empirical drag coefficient, (Schwing et al., 1996)
$\vec{v}_y$	Time series	$m\ s^{-1}$	North-South wind speed
$\lvert W \rvert$	Time series	$m\ s^{-1}$	Wind speed
ρ_{water}	1000	$kg\ m^{-3}$	Seawater density
d	$1.2\text{–}21{\cdot}10^{-6}$	$m\ s^{-1}$	Vertical diffusive mixing
b	0	$m\ s^{-1}$	Horizontal diffusive mixing, negligible relative to Ekman advection
MLD	15	m	Mixed Layer Depth
I_o	30–115	$W\ m^{-2}$	Light intensity at surface, (Brock, 1981)
k_w	0.067	m^{-1}	Light attenuation – seawater, (Newberger et al., 2003)
k_p	0.0095	$m^2\ mmol\ N^{-1}$	Light attenuation – phytoplankton, (Newberger et al., 2003)
i_p	20.6 (I) 6.9 (II) 22.2 (III) 3.6 (IV) 25.6 (V)	$mmol\ N\ m^{-3}$	Initial NO_3^- concentration for each sub-region; values for outer shelf surface (IV) and sub-surface (V) sub-regions are also used as oceanic boundary conditions. Values are from summer NH Line observations across central Oregon shelf (see Peterson and Keister, 2003 for NH Line details)

Merluccius productus, and sablefish, *Anoplopoma fimbria*) are secondary and tertiary producers of the benthic food web.

In the second analysis, ecosystem dynamics across a range of upwelling event durations were studied by driving the model under simulated upwelling time series. The central Oregon coast UI time-series for the 1967–2014 period (April–Sept.) was examined to determine the duration of individual upwelling events within the recent past and to create simulated upwelling time series. An upwelling event was defined as an uninterrupted period with a negative median daily UI value, and hence offshore Ekman transport of surface water. A relaxation event was defined as an uninterrupted period with zero or positive median daily UI, and onshore Ekman transport of surface water. Between 1967 and 2014, the mean duration of summer upwelling events off the central Oregon coast was 8.8 d (±11.5 d, 1 std. deviation) and the mean duration of a relaxation event was 2.7 d (±2.4 d) (Fig. 6). Simulated time series were created by overlaying an oscillating cycle of alternate upwelling event periods (3, 6, 9, 12, and 15 d) upon a seasonal upwelling/relaxation cycle (Fig. 7). The positive and negative amplitude range of the seasonal cycle was taken from the 1967–2014 UI time series, smoothed using a 40-day running mean. The daily positive and negative amplitude range was taken from the seasonally detrended time-series. Simulated time series were constructed such that cumulative volume transport rates from April–Sept. were similar: $7100\ m^3\ s^{-1}\ (100\ m)^{-1}$ oceanward for all upwelling events and $3800\ m^3\ s^{-1}\ (100\ m)^{-1}$ coastward for all downwelling events. Application of defined volumetric transport rates and upwelling event duration delimits the upwelling/downwelling duration ratios. Specifically, the mean upwelling/downwelling duration ratios (d/d) were 3/3, 6/5, 9/7, 12/9, and 15/12 for the 3, 6, 9, 12, and 15 d event time series, respectively. The model was run for 5 years under the simulated time series. Ecosystem response was measured as the biomasses of four indicator groups (copepods, forage fishes, invertebrate epifuana, semi-demersal fishes) averaged over the summer (July–Sept.) of the final simulation year.

3. Results

3.1. Phytoplankton and copepod grazer dynamics

From 432 alternate Michaelis–Menten models of phytoplankton nutrient uptake and growth, one model set (Appendix Table A11) was selected for use in all subsequent simulations of ecosystem behaviour under alternate upwelling conditions. The Pearson product-moment correlation between NH Line survey estimates of total phytoplankton biomass and corresponding model estimates for a given survey date (all seasons of years 1999–2013) and location (inner, mid, or outer shelf) is $r = 0.48$ ($n = 761$, $P < 0.01$). The correlation between NH Line estimates of total copepod biomass and corresponding model estimates (inner and outer shelf locations only) is $r = 0.48$ ($n = 664$, $P < 0.01$).

Comparisons of summer (July–Sept.) model and NH Line estimates at inner and outer shelf locations are also provided in Table 3 and Fig. 3. In terms of scale, the seasonal mean modelled and NH Line estimates of phytoplankton biomass are within 60% of each other. Phytoplankton size-class compositions are also in agreement over the inner shelf but diverge over the outer shelf, with the model estimating a higher proportion of smaller phytoplankton. However, note that the NH Line estimates were made under the assumption that the cellular Chl *a* content of the different phytoplankton size classes do not change with time nor with distance from the coast and the region of active upwelling. The modelled copepod biomass is consistently higher than estimated from the NH Line survey with no correction for net-avoidance. The seasonal model-to-observation comparisons have been restricted to the 2006–2013 period for consistency of the NH Line Chl *a* size-class sampling protocol.

3.2. Simulations of alternate upwelling strength

Figs. 4 and 5 show the effect of re-scaling the intensity (amplitude) of upwelling events upon four indicator groups: copepods, forage fishes, invertebrate epifuana, and semi-demersal fishes. Production rates and biomasses show dome-shaped relationships with upwelling intensity. Increasing upwelling strength leads to greater production for each of these groups as higher nutrient supply rates drive higher primary and consumer production that propagates through the food web (the left portion of the biomass vs. upwelling curves, Figs. 4 and 5). Increasing upwelling strength begins to have a detrimental effect on production when the physical export of plankton exceeds the capacity of phytoplankton to exploit higher nutrient supply rates and the capacity of zooplankton to exploit higher phytoplankton production (the right portion of the biomass vs. upwelling curves). Over the mid and outer shelf, net plankton production is supported by both local nutrient uptake by phytoplankton and by advective inputs of biomass. The optimum upwelling strength for all groups is, therefore higher with greater

Table 3
Comparison of the median summer (July–Sept., 1999–2013) NH Line survey and model-derived estimates of phytoplankton and copepod biomasses within the inner shelf (0–10 km) and outer shelf (30–50 km) zones. P_{tot} = biomass density of pooled phytoplankton size classes, and C_{tot} = total copepod biomass density (values in parentheses are the 25th and 75th percentiles of all values pooled across years). Correlation coefficients (r) are given for comparisons between survey estimates and corresponding model estimates for each survey date and cross-shelf location (across all seasons).

	Inner shelf (July–Sept.)				outer shelf (July–Sept.)				Whole shelf (full year)	
	NH Line		model		NH Line		model			
P_{tot} (mmole N m^{-3})	2.8	(1.3–5.6)	6.9	(6.1–7.6)	0.6	(0.4–1.4)	2.2	(1.7–3.0)	0.48*	761
C_{tot} (mmole N m^{-3})	0.3	(0.2–0.4)	1.6	(1.4–1.8)	0.1	(0.1–0.2)	0.7	(0.6–1.0)	0.48*	664

* $P < 0.01$.

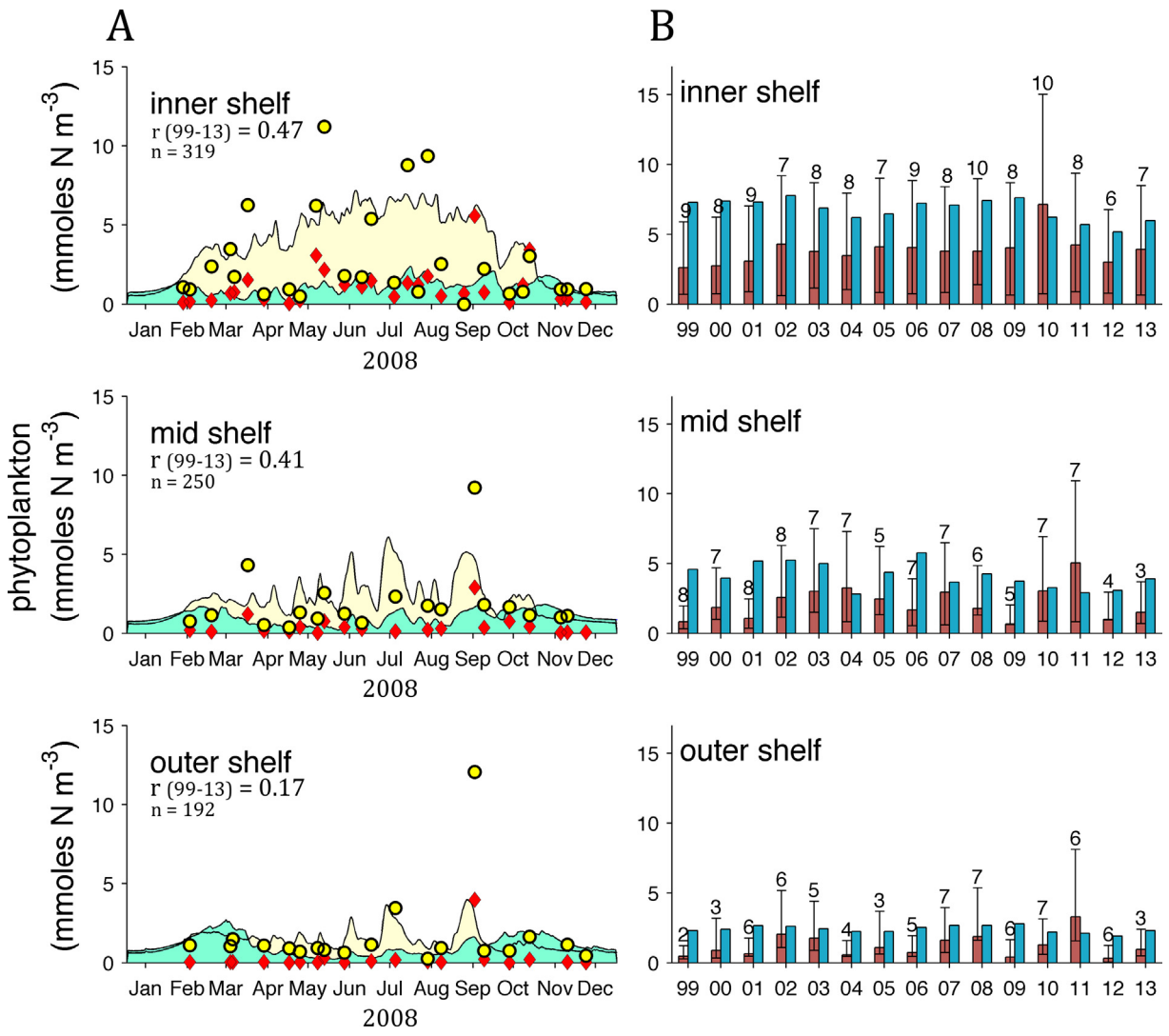

Fig. 3. Comparison of modelled phytoplankton biomass and estimates derived from NH Line observations. (A) One-year (2008) time series of modelled and NH Line estimates. Modelled P_L (diatoms): yellow curves; modelled P_S (flagellates): blue curves; NH Line P_L: yellow circles; NH Line P_S: red diamonds. The r-values and sample numbers represent correlations between NH Line estimates of total phytoplankton biomass and corresponding model estimates over years 1999–2013 (all values are significant at $P < 0.05$). (B) Summer (July–Sept.) means of modelled (blue bars) and NH Line-derived total phytoplankton biomass (red bars). Error bars represent ±1 standard deviation about observed means. Numbers above error bars are numbers of observations.

distance from the inner shelf where upwelling brings nutrient rich sub-surface waters into the euphotic zone (Fig. 4).

Higher rates of detritus and nutrient recycling also lead to greater production among both pelagic and demersal groups. Enhanced ammonium supply rates drive higher phytoplankton production and higher consumer production among all trophic levels and at all simulated upwelling strengths (as shown by the elevated curves in Fig. 5). The optimum upwelling strength occurs at a slightly lower level as recycling is increased. This is likely due to the lower proportion of ammonium production that is exported from a sub-region at lower upwelling levels (Figs. 6 and 7).

3.3. Simulations of alternate upwelling event duration

When the duration of individual upwelling events was shorter than the 9-day benchmark, the mean upwelling event duration from 1967 to 2014, the productivity and biomass of nearly every group increased. The strongest responses occurred within the inner

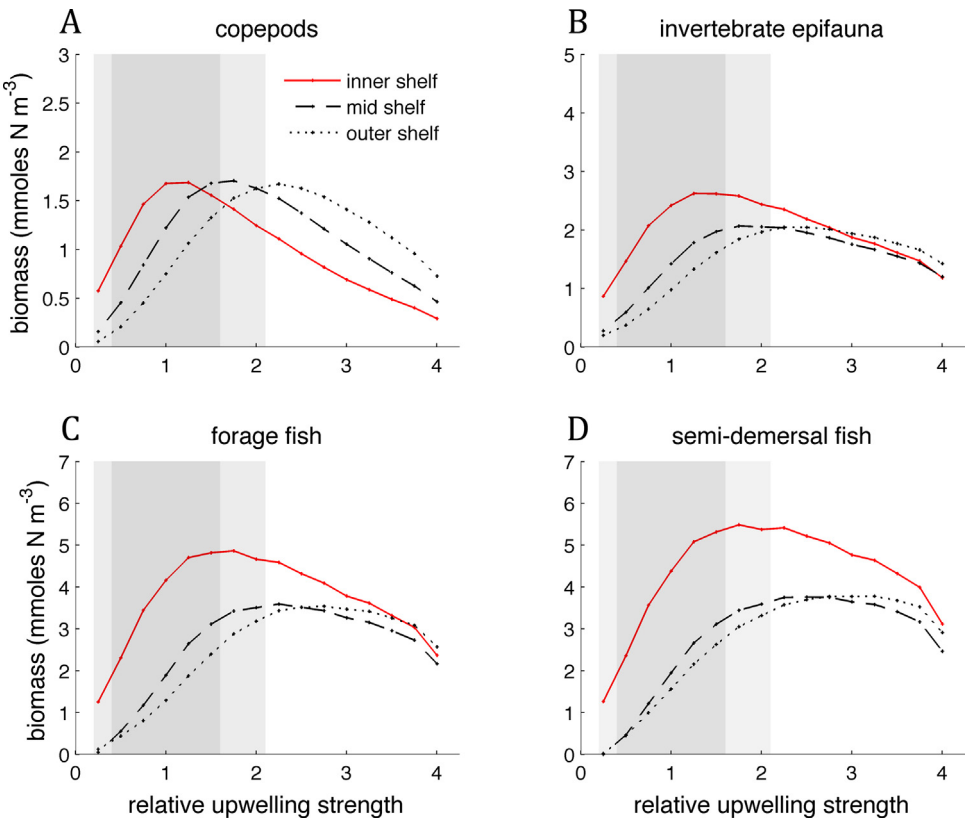

Fig. 4. Effect of re-scaling the amplitude of 2006–2010 upwelling events (relative upwelling strength = re-scaling by factors of 0.25–4×). Relaxation events were unaltered. Responses shown are final-year August biomasses of four indicator groups: (A) copepods, (B) invertebrate epifuana, (C) forage fish, (D) semi-demersal fish (note different *y*-axis scales). Solid red line: inner shelf; dashed line: mid shelf; dotted line: outer shelf. Dark shaded area represents the 25th–75th percentile range of upwelling event intensities across all 1967–2014 upwelling seasons (April–Sept.). Light shaded area represents the 10th–90th percentile range.

shelf zone, and the greatest changes occurred when upwelling events were shortened to 3 days (Table 4, Figs. 8 and 9). While the cumulative upwelling and downwelling volume transport rates were similar under the alternate event duration regimes, the transport of plankton biomass across the shelf was reduced during shorter upwelling events. This allowed for the continuity of larger phytoplankton and zooplankton grazer populations over the inner and mid shelf, which could better exploit enhanced nutrient input rates during upwelling events before nutrients and plankton were advected off the shelf. Longer event durations led to greater transport of plankton production across the shelf during upwelling events and reduced productivity of groups across all trophic levels within the inner and mid shelf ecosystems. The outer shelf ecosystem was much less sensitive to changing upwelling duration than were the inner and mid shelf ecosystems, except under shortest (3 d) upwelling event regime when the productivity of most groups increased by >10%. Among the higher trophic levels, most groups responded by roughly similar relative amounts. Benthic groups (benthic invertebrates and demersal fish) were slightly less sensitive to the more extreme shortening (i.e., 3-day events) of upwelling event duration. The strongest higher trophic level responses were again evident within the inner shelf region (Fig. 9).

Event duration also affected phytoplankton community composition (Fig. 8). Both diatom and flagellate biomasses were reduced within the inner shelf region under longer event duration regimes. This may again be attributed to greater transport of phytoplankton across the shelf. However, greater nitrate availability during prolonged upwelling events provided diatoms a competitive advantage over flagellates, leading to higher diatom/flagellate ratios within the inner and mid shelf regions as event durations increased (Fig. 8C). There was comparatively little change in either diatom or flagellate biomass within the outer shelf region.

We tested whether the model-predicted change towards a higher diatom-to-flagellate community composition under longer upwelling event conditions was evident within the 1999–2013 NH Line time series. A right-tailed Wilcoxon rank sum test was used to test the hypothesis that community size-class composition, the ratios of large to small phytoplankton concentrations (P_L/P_S) observed throughout the upwelling season (April–Sept.), did not differ among years of short and long event durations against the alternative that large phytoplankton were more abundant during years of long upwelling events. Over the 1967–2014 period (Fig. 6), NH Line observation years 2000, 2007, 2008, and 2009 were within the lower 25th percentile of mean summer upwelling event durations (<7.4 d) and years 1999, 2002, and 2006 were within the upper 75th percentile (>11.0 d). Phytoplankton concentrations were based directly upon surface chlorophyll measurements and not converted to nitrogen equivalents. Two distinct periods were compared preceding and following a change in plankton filtration protocol; phytoplankton were divided into <10 μm and ≥10 μm size fractions through 2005 and into <5 μm and ≥5 μm size fractions since 2006 (W. Peterson, pers. comm.). Over the inner shelf, the P_L/P_S ratio was significantly higher during longer event duration years (Table 5) in both filtration protocol periods. There was no significant difference in size composition over the mid shelf and outer shelf regions.

4. Discussion

Comparative studies of ecosystem structure and dynamics using energy or tracer budgets are useful for highlighting the

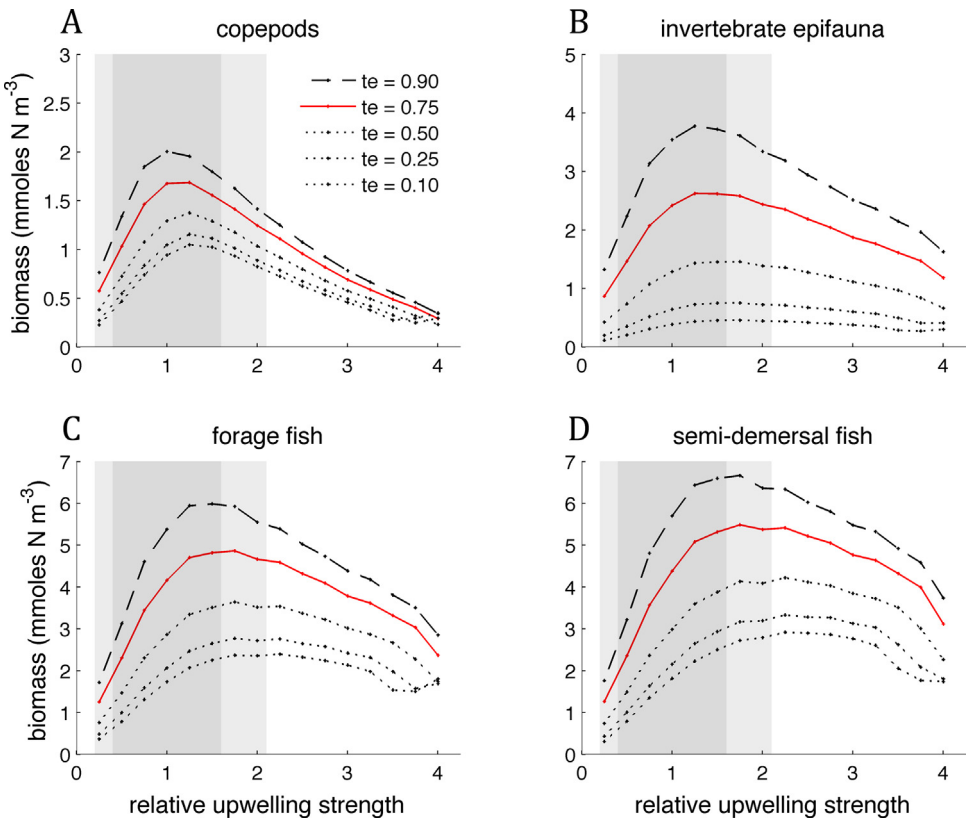

Fig. 5. Effects re-scaling the amplitude of 2006–2010 upwelling events under alternate nutrient recycling rate assumptions within the inner shelf. Responses shown are final-year August biomasses of four indicator groups: (A) copepods, (B) invertebrate epifuana, (C) forage fish, (D) semi-demersal fish (note different *y*-axis scales). Solid red line: benthic detritus recycling fraction *te* = 0.75; dashed line: recycling fraction *te* = 0.9; dotted lines: recycling fraction *te* = 0.5, 0.25, and 0.1. Dark shaded area represents the 25th–75th percentile range of upwelling event intensities across all 1967–2014 upwelling seasons (April–Sept.). Light shaded area represents the 10th–90th percentile range.

underlying mechanics that drive and moderate ecosystem variability. Food web model-based studies generally focus on the evolution of trophic relationships over time following the application of an externally applied pressure (e.g., fishing), but they do not incorporate the physical dynamics of the ecosystem into the inherent model structure. Consideration of the physical context of ecosystem structure is especially important for studying the role of lower trophic dynamics on the upper food web and fishery production. Physical fluxes drive the input of nutrients to the system, the export of production from the system, and the strength of benthic-pelagic coupling and nutrient recycling via bioturbation, diagenesis, nitrification and denitrification (Ruardij and Raaphorst, 1995). The nutrient recycling rate is a defining feature distinguishing different ocean ecosystems. If ecosystem response to climatic or to anthropogenic perturbation is a function of the relative importance of ecologically moderated nutrient recycling vs. the physically moderated external nutrient supply rate, then water residence time-scale becomes an important descriptor of ecosystem dynamics. For eastern boundary current upwelling ecosystems like the Northern California Current residence times are short, on the order of 10–30 d (Steele and Ruzicka, 2011), and we expect variable physical flux and nutrient supply rates to drive high levels or interannual variability.

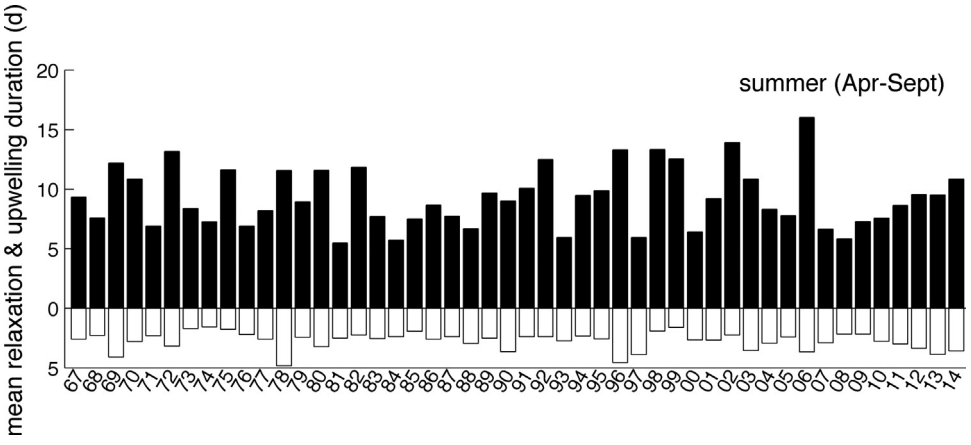

Fig. 6. Time series of summer upwelling (black) and relaxation (white) event durations off the central Oregon coast.

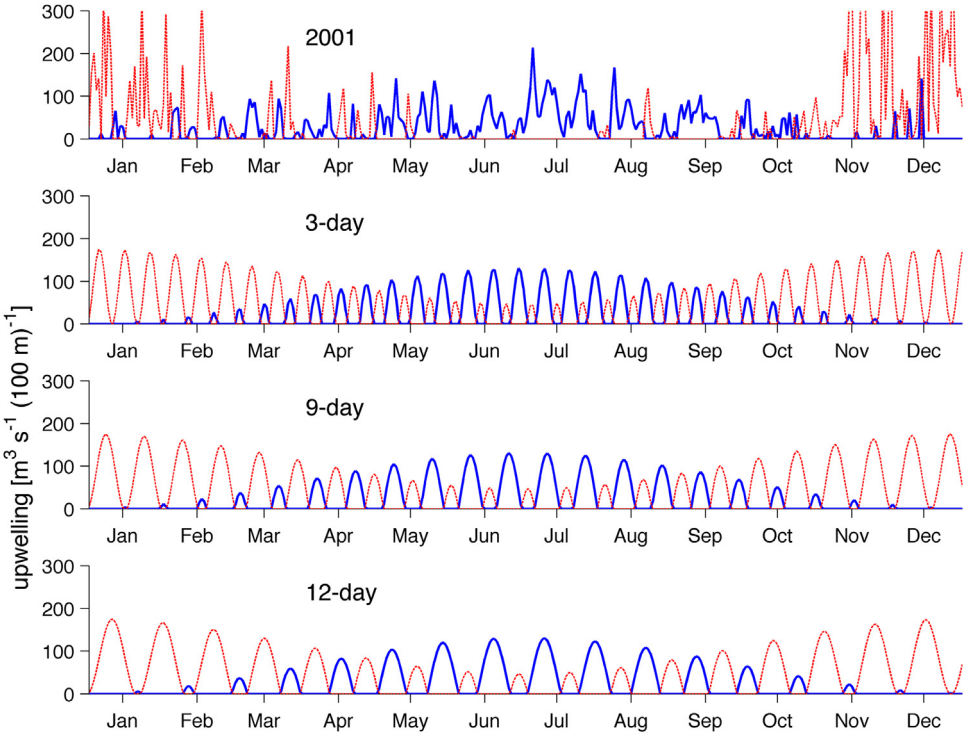

Fig. 7. Upwelling driver time series used to simulate effects of alternate upwelling event duration. Blue solid lines represent upwelling events, and red dashed lines represent downwelling and relaxation events. In the driver time series, upwelling events have a negative sign.

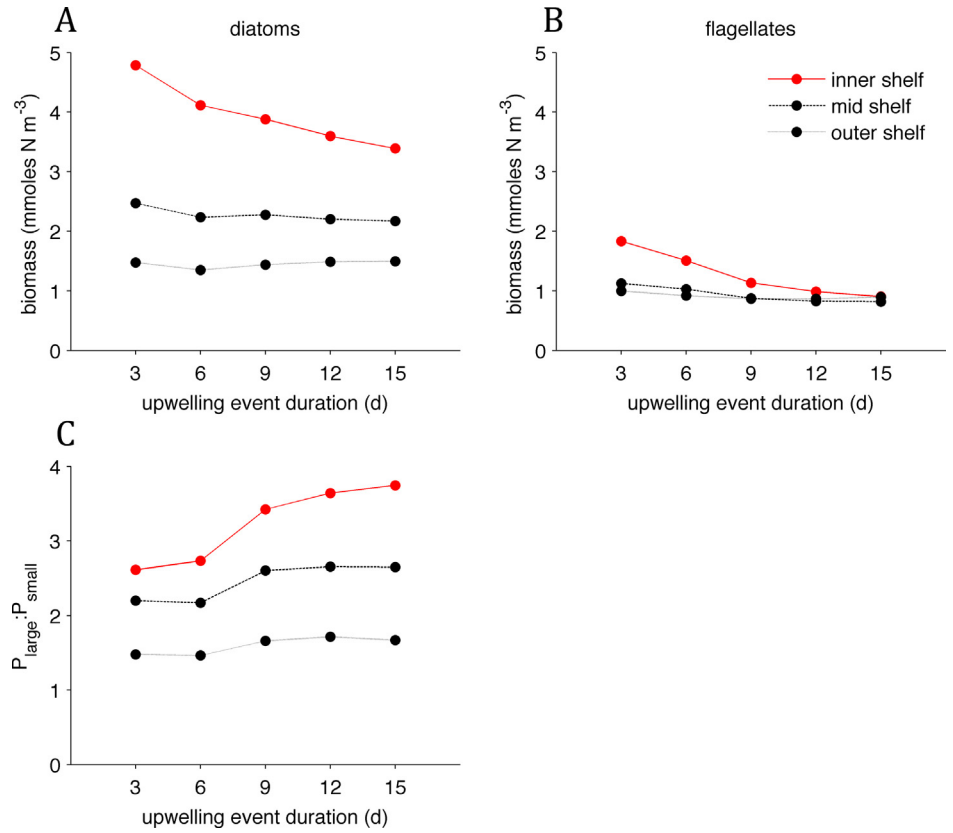

Fig. 8. Effects of alternate upwelling event duration upon August biomasses of two phytoplankton size classes, (A) diatoms and (B) flagellates, and upon (C) the diatom/flagellate ratio at inner, mid, and outer shelf locations. Solid red line: inner shelf; solid black line: mid shelf; dotted black line: outer shelf.

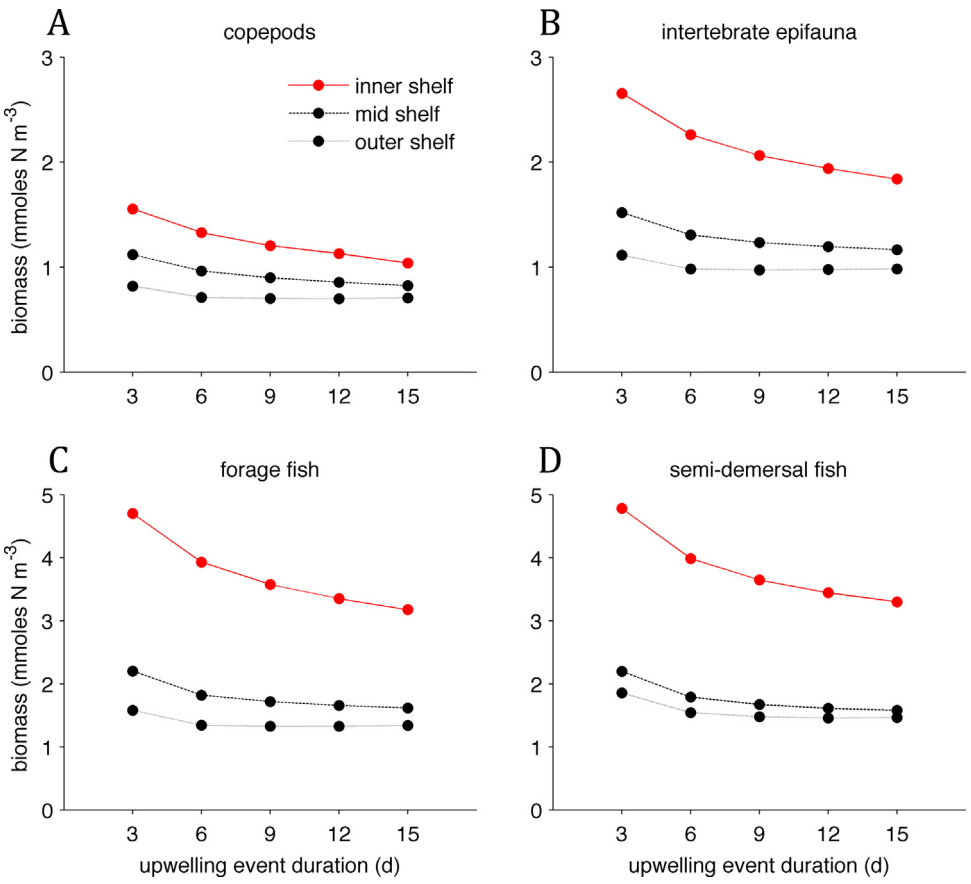

Fig. 9. Effects of alternate upwelling event duration upon August biomasses of four indicator groups at inner, mid, and outer shelf locations: (A) copepods, (B) invertebrate epifuana, (C) forage fish, (D) semi-demersal fish. Solid red line: inner shelf; solid black line: mid shelf; dotted black line: outer shelf.

For large semi-enclosed systems like the North Sea residence times are long, on the order of 300–500 days (Otto et al., 1990), and we expect that recycling may be more important for defining ecosystem dynamics than physical flux rates across ecosystem boundaries (Steele and Ruzicka, 2011).

Physically coupled, end-to-end models are being developed specifically to address this issue. However, the incorporation of 3-dimensional physical processes within a trophic model adds a high level of complexity to model development and requires greater computational effort. This impedes rapid or casual exploratory analyses. Our goal was to build an intermediate complexity E2E model that integrates two-dimensional physical advection and mixing processes with a food web model that tracks energy (biomass) flow from nutrient input, to the highest trophic levels, and back to recycled detritus and nutrients. Construction of such models may be greatly advanced by taking advantage of the large set of ECOPATH models describing trophic network relationships for diverse ecosystems around the world (www.ecopath.org). The physical model is simplified by not attempting to resolve ephemeral or detailed physical structures such as eddies or fronts but instead concentrating on major nutrient and biomass exchanges across lateral and vertical boundaries. Correspondingly, the model developed here considers large (regional) along-isobath spatial scales in the expectation that averaged over large alongshore distances, systems are reasonably two-dimensional (e.g., Lentz, 1987). That is, we have assumed that alongshore fluxes into the model balance alongshore fluxes out of the model.

Application of this model platform to the Northern California Current (NCC) allowed us to look at ecosystem sensitivity and response to variability in upwelling characteristics. Upwelling-supported phytoplankton production over the continental shelf is a balance between the nutrient supply rate to surface waters and Ekman transport of surface waters and plankton biomass off the shelf. Ecosystem productivity is hypothesized to have a non-linear, dome-shaped relationship with upwelling intensity (Botsford et al., 2003). Primary and secondary productivity increases as phytoplankton take advantage of the increasing nutrient supply rate. When Ekman transport rates begin to exceed the ability of the phytoplankton community to utilize the increased nutrient supply rate, production rates decline with increasing upwelling intensity. An example of this dome-shaped relationship has been observed between upwelling indices and phytoplankton and euphausiid abundances off northern California (Garcia-Reyes et al., 2014) and the recruitment of coho salmon to Oregon coastal rivers (Rupp et al., 2012). This mechanism is different from Cury and Roy's (1989) hypothesis for an optimum environmental window for fish recruitment in Ekman upwelling systems. Cury and Roy attributed observed trends of reduced fish production under intense upwelling to the disruptive role of turbulence upon plankton patch formation. Botsford et al. (2003) attribute declining productivity under intense upwelling to increased loss of plankton production from the shelf through horizontal advection. However, both processes may play a role at the same time.

Our model simulations also showed dome-shaped relationships between upwelling strength and biomass across all trophic levels. With greater distance from the coast, maximum potential production rates were realized at greater upwelling intensities (Fig. 4). The physical export rate of passive particles during a typical NCC upwelling season can exceed the production rate of the more slowly growing zooplankton groups, making the populations unsustainable without the action of behavioural retention mechanisms (Steele and Ruzicka, 2011). Diel and ontogenetic vertical

Table 4
Percent change in simulated summer productivity (July–Sept.) under alternate upwelling event durations relative to a 9-day event benchmark.

		3 d	6 d	12 d	15 d
Inner shelf	Primary prod: diatoms	23%	6%	−7%	−13%
	Primary prod: flagellates	62%	33%	−13%	−20%
	Mesozooplankton	29%	11%	−7%	−14%
	Macrozooplankton	29%	10%	−6%	−12%
	Euphausiids	31%	12%	−7%	−13%
	Gelatinous zooplankton	28%	9%	−6%	−12%
	Large jellyfish	26%	7%	−3%	−8%
	Squid	32%	11%	−7%	−12%
	Forage fish	31%	10%	−6%	−11%
	Piscivorous fish	31%	9%	−6%	−9%
	Benthic invertebrates	29%	10%	−6%	−11%
	Semi-demersal fish	31%	9%	−6%	−9%
	Demersal fish	28%	8%	−5%	−9%
	Seabirds	33%	11%	−7%	−12%
	Mammals	32%	10%	−6%	−10%
	Fisheries (constant effort)	29%	10%	−6%	−10%
Mid shelf	Primary prod: diatoms	9%	−2%	−3%	−5%
	Primary prod: flagellates	28%	18%	−5%	−6%
	Mesozooplankton	24%	7%	−5%	−8%
	Macrozooplankton	22%	6%	−3%	−6%
	Euphausiids	16%	4%	−2%	−5%
	Gelatinous zooplankton	27%	8%	−5%	−8%
	Large jellyfish	32%	8%	−5%	−9%
	Squid	29%	7%	−4%	−6%
	Forage fish	28%	6%	−4%	−6%
	Piscivorous fish	32%	7%	−4%	−6%
	Benthic invertebrates	23%	6%	−3%	−6%
	Semi-demersal fish	31%	7%	−4%	−6%
	Demersal fish	27%	6%	−3%	−5%
	Seabirds	40%	9%	−5%	−8%
	Mammals	38%	8%	−4%	−7%
	Fisheries (constant effort)	25%	6%	−3%	−6%
Outer shelf	Primary prod: diatoms	2%	−6%	3%	4%
	Primary prod: flagellates	15%	6%	0%	3%
	Mesozooplankton	16%	1%	0%	1%
	Macrozooplankton	14%	1%	0%	1%
	Euphausiids	6%	−2%	2%	3%
	Gelatinous zooplankton	22%	3%	−1%	−1%
	Large jellyfish	33%	6%	−3%	−4%
	Squid	19%	1%	1%	2%
	Forage fish	19%	1%	0%	1%
	Piscivorous fish	26%	5%	−1%	−1%
	Benthic invertebrates	15%	1%	0%	1%
	Semi-demersal fish	26%	5%	−1%	−1%
	Demersal fish	23%	5%	−1%	−1%
	Seabirds	29%	2%	0%	1%
	Mammals	29%	4%	−1%	0%
	Fisheries (constant effort)	22%	5%	−1%	−1%

Table 5
Comparison of phytoplankton community size-class composition along NH Line stations in years of long mean upwelling event duration (1999, 2002, 2006) and years of short event duration (2000, 2007, 2008, 2009). Surface phytoplankton concentrations are based upon Chl *a* (mg Chl *a* m^{-3}). Large (P_L) and small (P_S) phytoplankton were divided into <10 μm and ≥ 10 μm size fractions (1999–2005) and into <5 μm and ≥5 μm size fractions (2006–2013).

		Inner shelf (NH 5)		Mid shelf (NH 15)		Outer shelf (NH 25)	
	Year group	P_L/P_S	*n*	P_L/P_S	*n*	P_L/P_S	*n*
1999–2005	Long duration	**6.8** (4.9–17.2)[a]	18	3.6 (0.7–8.3)	15	2.1 (0.6–6.1)	4
(P_L Chl *a* ≥10 μm)	Short duration	**2.0** (0.9–6.7)	11	0.2 (0.2–0.7)	7	–	0
2006–2013	Long duration	**1.4** (1.0–2.7)[a]	18	1.0 (0.2–1.3)	12	0.1 (0.1–0.6)	11
(P_L Chl *a* ≥5 μm)	Short duration	**0.9** (0.5–1.7)	56	0.8 (0.4–1.0)	39	0.4 (0.1–0.8)	41

[a] P_L/P_S ratio is significantly higher during long upwelling event duration years than during short duration years ($P < 0.05$) as determined by right-tailed Wilcoxon rank sum test.

migration are recognized mechanisms by which zooplankton populations may minimize time spent in the surface layer, reducing or reversing offshore transport (Batchelder et al., 2002; Lamb and Peterson, 2005). Greater zooplankton resistance to advection leads to greater fish production and fishery yield at a given upwelling rate and greater potential fish production rates as upwelling intensity increased (Steele and Ruzicka, 2011). Higher rates of detritus and nutrient recycling in the present model simulations also lead to greater potential production rates, at optimum upwelling intensities, among both pelagic and benthic groups (Fig. 5).

How are local upwelling dynamics expected to change in the future within the framework of a globally changing climate, and what will be the consequences to NCC ecosystem productivity and structure? Bakun (1990) speculated that global warming would

lead to steeper temperature gradients between the ocean and the land, leading to greater alongshore wind-stress and increased upwelling intensity within eastern boundary current ecosystems. While model projections of upwelling conditions under future climate change scenarios have been inconsistent (e.g., Snyder et al., 2003; Wang et al., 2015), a meta-analysis of published wind-trend studies (Sydeman et al., 2014) show that seasonal alongshore winds have indeed been increasing among the major eastern boundary current upwelling ecosystems (California, Humboldt, Canary, and Benguela Currents) over the past half-century. Based on observed wind data, the mean seasonal upwelling strength within the NCC has been gradually increasing. At the northern extent of the NCC, off southern Vancouver Island (48.8° N), the mean daily upwelling rate has increased at a rate of ~ 0.3% per year over the past half-century (Foreman et al., 2011). At the southern extent of the NCC, off northern California (41.8° N), the mean daily upwelling rate has increased at a rate of ~ 4% per year over the past quarter-century (García-Reyes and Largier, 2010).

Our model simulations then suggest that as seasonal upwelling intensifies, we will see increasing NCC ecosystem productivity in the future. Most individual upwelling events over the 1967–2014 upwelling season (April–Sept.) fall within the portion of the intensity vs. productivity curve where stronger upwelling drives stronger production (Fig. 4). However, the broad distribution of upwelling event intensities suggest that during the strongest events the NCC already realizes the negative effects of lost plankton production via Ekman export. As the proportion of strong upwelling events increases beyond current conditions, overall ecosystem productivity will decline (Fig. 4). Rupp et al. (2012) report reduced recruitment of coho salmon to Oregon coastal rivers in years when the mean summer (July–Sept.) upwelling strength exceeds an optimum ~50 $m^3\ s^{-1}\ (100\ m)^{-1}$; for reference, the upper 75th percentile of daily July–Sept. 1967–2014 upwelling strengths exceeds this value at 61 $m^3\ s^{-1}\ (100\ m)^{-1}$.

Besides variability in upwelling intensity, seasonal wind-driven upwelling is episodic. The alteration of upwelling and relaxation events plays an important role in the strength and cross-shelf position of phytoplankton blooms (Wilkerson et al., 2006), the retention of planktonic groups on the shelf, and the recruitment of oceanic larvae transported back to the coast (Barth et al., 2007). Alteration of upwelling and relaxation events serves to increase the transit time of plankton across the shelf, allowing increased time for development of phytoplankton blooms and time for grazers to utilize this resource over the inner shelf (Botsford et al., 2006). Under identical levels of cumulative upwelling, shorter and more frequent upwelling events would lead directly to higher primary production and higher upper trophic level production over the inner and mid continental shelf. Our five simulated upwelling time series were created such that each had similar cumulative upwelling over the April–Sept. season, but the time series with shorter upwelling event durations had the higher ecosystem production rates.

The duration of wind-driven summer upwelling events in the NCC occurs on two time scales, 20-day oscillations in the position of the jet stream and 2- to 6-day "weather-band" fluctuations (Largier et al., 1993; Bane et al., 2007). Between 1967 and 2014, we found that the median upwelling event duration was 9 days and the median downwelling event duration was 3 days (Fig. 6). Differential warming of the Arctic relative to the whole of the northern hemisphere is predicted to lead to slower oscillations in jet stream position and prolonged weather conditions (Francis and Vavrus, 2012), and this could mean longer duration upwelling and relaxation events. Iles et al. (2012) analyzed trends in the event-scale characteristics within the California Current. Upwelling events in the California Current have become stronger, less frequent, and longer in duration over the past four decades. In the NCC (45° N), the mean upwelling event duration has increased by 26% (Iles et al., 2012).

From our model simulations (Figs. 8 and 9), longer upwelling events in the future would imply an overall reduction of ecosystem productivity and a shift towards mid and outer shelf production, or a lesser reduction of productivity away from the coast. All trophic levels would experience these effects. The long period over which these simulations were run, 5 years, was sufficient for groups across all trophic levels to reach new, stable biomasses. All functional groups showed responses upon a similar scale, reflecting the decline in total production at the base of the food web. There were some differences among mid and upper trophic level group responses. For example, benthic groups supported by the detritus production (benthic invertebrates and demersal fish) were slightly less sensitive to the more extreme changes (i.e., 3-day events) in upwelling event duration. This perhaps reflects the fact that, in the model, all unconsumed production in the whole ecosystem becomes homogenized into a single benthic detritus pool that supports the benthic food web, and most fine differentiations between alternate primary and secondary production pathways are lost.

There was also a shift in the composition of the phytoplankton community towards greater diatom production relative to flagellates, especially inshore (Fig. 8C). This predicted shift was supported by ocean observations (Section 3.3). We did not investigate the consequences of this, but a shift towards a larger-sized phytoplankton community would imply a shift towards a larger-sized grazer community, fewer trophic steps between primary and fish production, and a more efficient ecosystem. However, we speculate that a less diverse phytoplankton community could mean a less diverse mixture of fixed essential fatty acids with lower food quality per unit of biomass (e.g., El-Sabaawi et al., 2009) propagating up the food web.

5. Conclusion

Our hope is that the intermediate complexity end-to-end model platform developed here will complement more complex "virtual world" models such as ATLANTIS (Brand et al., 2007; Link et al., 2010) through their relative ease of use, portability between systems, and the clarity they provide for revealing the underlying mechanisms of observed dynamics. The use of models simple enough to allow comparisons among regions but sufficiently realistic to allow testing against data, while necessarily limited, allow ecosystem control concepts to be explored within ecologically interesting and societally important arenas. Our application to the Northern California Current allowed us to simulate ecosystem response to upwelling conditions that are expected to change into the future with the progression of global climate change, e.g., upwelling strength and the duration of upwelling/relaxation events. Applications of this model platform are being extended to comparative studies of the Georges Bank, Gulf of Alaska, and North Sea ecosystems. With a comparison of these ecosystems under identical physical frameworks, we hope to evaluate the relative roles of the physical setting against the trophic network structure in the dynamics of diverse coastal ecosystems.

Acknowledgements

We thank J. Fisher (Oregon State University) and W. Peterson (NOAA NWFSC) for providing the Newport Hydrographic dataset. This work was supported by grant OCE 1258667 to KHB, FB, and DHJ and grant OCE 1416905 to JJR from the US National Science Foundation.

Appendix A. Supplementary data

Supplementary data associated with this article can be found, in the online version, at http://dx.doi.org/10.1016/j.ecolmodel.2016.01.018.

References

Ainsworth, C.H., Samhouri, J.F., Busch, D.S., Cheung, W.W.L., Dunne, J., Okey, T.A., 2011. Potential impacts of climate change on Northeast Pacific marine foodwebs and fisheries. ICES J. Mar. Sci. 68, 1217–1229.

Bakun, A., 1990. Global climate change and intensification of coastal ocean upwelling. Science 247, 198–201.

Ballerini, T., Hofmann, E.E., Ainley, D.G., Daly, K., Marrari, M., Ribic, C.A., Smith, W.O., Steele, J.H., 2014. Productivity and linkages of the food web of the southern region of the western Antarctic Peninsula continental shelf. Prog. Oceanogr. 122, 10–29.

Bane, J.M., Spitz, Y.H., Letelier, R.M., Peterson, W.T., 2007. Jet stream intraseasonal oscillations drive dominant ecosystem variations in Oregon's summertime coastal upwelling system. PNAS 104, 13262–13267.

Barth, J.A., Menge, B.A., Lubchenco, J., Chan, F., Bane, J.M., Kirincich, A.R., McManus, M.A., Nielsen, K.J., Pierce, S.D., Washburn, L., 2007. Delayed upwelling alters nearshore coastal ocean ecosystems in the Northern California Current. Proc. Natl. Acad. Sci. U. S. A. 104, 3719–3724.

Batchelder, H.P., Edwards, C.A., Powell, T.M., 2002. Individual-based models of copepod populations in coastal upwelling regions: implications of physiologically and environmentally influenced diel vertical migration on demographic success and nearshore retention. Prog. Oceanogr. 53, 307–333.

Bograd, S.J., Schroeder, I., Sarkar, N., Qiu, X., Sydeman, W.J., Schwing, F.B., 2009. Phenology of coastal upwelling in the California Current. Geophys. Res. Lett. 36, L01602.

Botsford, L.W., Lawrence, C.A., Dever, E.P., Hastings, A., Largier, J., 2003. Wind strength and biological productivity in upwelling systems: an idealized study. Fish. Oceanogr. 12, 245–259.

Botsford, L.W., Lawrence, C.A., Dever, E.P., Hastings, A., Largier, J., 2006. Effects of variable winds on biological productivity on continental shelves in coastal upwelling systems. Deep-Sea Res. II 53, 3116–3140.

Brand, E.J., Kaplan, I.C., Harvey, C.J., Levin, P.S., Fulton, E.A., Hermann, A.J., Field, J.C., 2007. A Spatially Explicit Ecosystem Model of the California Current's Food Web and Oceanography.

Brock, T.D., 1981. Calculating solar radiation for ecological studies. Ecol. Model. 14, 1–19.

Chan, A.T., 1980. Comparative physiological study of marine diatoms and dinoflagellates in relation to irradiance and cell size. II. Relationship between photosynthesis, growth, and carbon/chlorophyll a ratio. J. Phycol. 18, 428–432.

Christensen, V., Walters, C.J., 2004. Ecopath with Ecosim: methods, capabilities and limitations. Ecol. Model. 172, 109–139.

Cury, P., Roy, C., 1989. Optimal environmental window and pelagic fish recruitment success in upwelling areas. Can. J. Fish. Aquat. Sci. 46, 670–680.

Dickson, M.L., Wheeler, P.A., 1995. Nitrate uptake rates in a coastal upwelling regime: a comparison of PN-specific, absolute, and Chl *a*-specific rates. Limnol. Oceanogr. 40, 533–543.

Du, X., Peterson, W., O'Higgins, L., 2015. Interannual variations in phytoplankton community structure in the northern California Current during the upwelling seasons of 2001–2010. Mar. Ecol. Prog. Ser. 519, 75–87.

El-Sabaawi, R., Dower, J.F., Kainz, M., Mazumder, A., 2009. Interannual variability in fatty acid composition of the copepod Neocalanus plumchrus in the Strait of Georgia, British Columbia. Mar. Ecol. Prog. Ser. 382, 151–161.

Fisher, J.P., Pearcy, W.G., 1988. Growth of juvenile coho salmon (*Oncorhynchus kisutch*) off Oregon and Washington, USA, in years of differing coastal upwelling. Can. J. Fish. Aquat. Sci. 45, 1036–1044.

Foreman, M.G.G., Pal, B., Merryfield, W.J., 2011. Trends in upwelling and downwelling winds along the British Columbia shelf. J. Geophys. Res., 116, http://dx.doi.org/10.1029/2011JC006995.

Francis, J.A., Vavrus, S.J., 2012. Evidence linking Arctic amplification to extreme weather in mid-latitudes. Geophys. Res. Lett., 39, http://dx.doi.org/10.1029/2012GL051000.

Fulton, E., Smith, A., Johnson, C., 2004. Biogeochemical systems models I: IGBEM – a model of marine bay ecosystems. Ecol. Model. 174, 267–307.

Gaichas, S., Skaret, G., Falk-Petersen, J., Link, J.S., Overholtz, W., Megrey, B.A., Gjosaeter, H., Stockhausen, W.T., Dommasnes, A., Friedland, K.D., Aydin, K., 2009. A comparison of community and trophic structure in five marine ecosystems based on energy budgets and system metrics. Prog. Oceanogr. 81, 47–62.

García-Reyes, M., Largier, J., 2010. Observations of increased wind-driven coastal upwelling off central California. J. Geophys. Res.: Oceans 115, C04010.

Garcia-Reyes, M., Largier, J.L., Sydeman, W.J., 2014. Synoptic-scale upwelling indices and predictions of phyto- and zooplankton populations. Prog. Oceanogr. 120, 177–188.

Huyer, A., 1983. Coastal upwelling in the California Current. Prog. Oceanogr. 12, 259–284.

Iles, A., Gouhier, C.T.C., Menge, B.A., Stewart, J.S., Haupt, A.J., Lynch, M.C., 2012. Climate-driven trends and ecological implications of event-scale upwelling in the California Current System. Glob. Change Biol. 18, 783–796.

Lamb, J., Peterson, W.T., 2005. Ecological zonation of zooplankton in the COAST study region off Central Oregon in June and August 2001 with consideration of retention mechanisms. J. Geophys. Res. C. Oceans 110, C10S15.

Largier, J.L., Magnell, B.A., Winant, C.D., 1993. Subtidal circulation over the Northern California shelf. J. Geophys. Res. 98, 18147–18179.

Lentz, S.J., 1987. A heat budget for the northern California shelf during CODE 2. J. Geophys. Res. 92, 14491–14509.

Link, J.S., Fulton, E.A., Gamble, R.J., 2010. The north-east US application of ATLANTIS: a full system model exploring marine ecosystem dynamics in a living marine resource context. Prog. Oceanogr. 87, 214–234.

Newberger, P.A., Allen, J.S., Spitz, Y.H., 2003. Analysis and comparison of three ecosystem models. J. Geophys. Res. C. Oceans 108, http://dx.doi.org/10.1029/2001JC001182.

Otto, L., Zimmerman, J., Furnes, G., Mork, M., Soertre, R., Becker, G., 1990. Review of the physical oceanography of the North Sea. Netherlands J. Sea Res. 26, 161–238.

Pauly, D., Christensen, V., Walters, C., 2000. Ecopath, Ecosim, and Ecospace as tools for evaluating ecosystem impact of fisheries. ICES J. Mar. Sci. 57, 697–706.

Peterson, W.T., Miller, C.B., 1975. Year-to-year variations in the planktonology of the Oregon upwelling zone. Fish. Bull. 73, 642–653.

Peterson, W.T., Keister, J.E., 2003. Interannual variability in copepod community composition at a coastal station in the northern California Current: a multivariate approach. Deep Sea Res. (Part II: Top. Stud. Oceanogr.) 50, 2499–2517.

Peterson, W.T., Keister, J.E., Feinberg, L.R., 2002. The effects of the 1997–99 El Nino/La Nina events on hydrography and zooplankton off the central Oregon coast. Prog. Oceanogr. 54, 381–398.

Ruardij, P., Raaphorst, W., 1995. Benthic nutrient regeneration in the ERSEM ecosystem model of the North Sea. Netherlands J. Sea Res. 33, 453–483.

Rupp, D.E., Wainwright, T.C., Lawson, P.W., Peterson, W.T., 2012. Marine environment-based forecasting of coho salmon (*Oncorhynchus kisutch*) adult recruitment. Fish. Oceanogr. 21, 1–19.

Ruzicka, J.J., Steele, J.H., Ballerini, T., Gaichas, S.K., Ainley, D.G., 2013. Dividing up the pie: whales, fish, and humans as competitors. Prog. Oceanogr. 116, 207–219.

Ruzicka, J.J., Brodeur, R.D., Emmett, R.L., Steele, J.H., Zamon, J.E., Morgan, C.A., Thomas, A.C., Wainwright, T.C., 2012. Interannual variability in the Northern California Current food web structure: changes in energy flow pathways and the role of forage fish, euphausiids, and jellyfish. Prog. Oceanogr. 102, 19–41.

Ruzicka, J.J., Wainwright, T.C., Peterson, W.T., 2011. A simple plankton model for the Oregon upwelling ecosystem: sensitivity and validation against time-series ocean data. Ecol. Model. 222, 1222–1235.

Schwing F.B., O'Farrell, M., Steger, J.M., Baltz, K., 1996. Coastal Upwelling Indices West Coast of North America 1946–95. NOAA-TM-NMFS-SWFSC-231, SWFSC.

Snyder, M.A., Sloan, L.C., Diffenbaugh, N.S., Bell, J.L., 2003. Future climate change and upwelling in the California Current. Geophys. Res. Lett., 30, http://dx.doi.org/10.1029/2003GL017647.

Steele, J., Ruzicka, J.J., 2011. Constructing end-to-end models using ECOPATH data. J. Mar. Syst. 87, 227–238.

Steele, J.H., 2009. Assessment of some linear food web methods. J. Mar. Syst. 76, 186–194.

Strub, P., Allen, J.S., Huyer, A., Smith, R., Beardsley, R., 1987. Seasonal cycles of currents, temperatures, winds, and sea level over the Northeast Pacific continental shelf: 35° N to 48° N. J. Geophys. Res. 92, 1507–1526.

Sydeman, W.J., Garciía-Reyes, M., Schoeman, D.S., Rykaczewski, R.R., Thompson, S.A., Black, B.A., Bograd, S.J., 2014. Climate change and wind intensification in coastal upwelling ecosystems. Science 345, 77–80.

Treasure, A., Ruzicka, J., Moloney, C., Gurney, L., Ansorge, I., 2015. Land-sea interactions and consequences for sub-Antarctic marine food webs. Ecosystems 18, 752–768.

Wang, D., Gouhier, T.C., Menge, B.A., Ganguly, A.R., 2015. Intensification and spatial homogenization of coastal upwelling under climate change. Nature 518, 390–394.

Wilkerson, F.P., Lassiter, A.M., Dugdale, R.C., Marchi, A., Hogue, V.E., 2006. The phytoplankton bloom response to wind events and upwelled nutrients during the CoOP WEST study. Deep Sea Res. II 53, 3023–3048.